SVPWM-Based Three-Level Z Source Inverter for Grid-Connected Photovoltaic with Battery Storage Using Bidirectional DC-DC Converter

Ahmed Benfatah¹, Noureddine Henini², Abdelkader Morsli³

¹ "Laboratoire des systems électriques avancés", University of Medea, 26000, Medea, Algeria

Received: 17-04-2024 Accepted: 24-09-2024

This paper presents a Z-source inverter for a grid-connected photovoltaic (PV) producing system to achieve a one stage buck-boost (as per the solar variation). Between the DC voltage source (containing the PV array and a bidirectional buck-boost system) and the neutral-point clamped (NPC) inverter, a single LC impedance network is employed. We suggested a suitable SVPWM technique based on three-level single Z-source inverters, which includes vector region judgment, send order determination, and synthetic time computation. It is possible to accomplish inductive voltage boosting by correctly inserting the shoot-through vectors, while also providing acceptable output performance with a correct volt-second average. The PV array output voltage is adjusted and maximum power point tracking (MPPT) is obtained by adjusting the shoot-through duty cycle. Simulation findings validate the theoretical notions stated. **Keywords:** photovoltaic (PV), neuro-fuzzy controller, z-source inverter (ZSI), three-level (NPC), (SVPWM), bidirectional converter, D-STATCOM, battery.

1. Introduction

Grid-connected photovoltaic (PV) power conditioning systems have attracted significant interest for their dual functionality (Zha et al., 2021)-(Mahmud et al., 2021): they can supply active power generated by PV arrays to the utility grid and enhance power quality by filtering out unwanted harmonics and compensating for reactive power demand from nonlinear loads. Power converters in PV systems convert the direct current (DC) output from PV panels to alternating current (AC), enabling easy integration with the grid or direct

²Renewable Energy and Materials Laboratory, University of Medea, Medea 26000, Algeria ³Electrical Engineering and Automation Research Laboratory (LREA), University of Medea, Medea, Algeria

powering of local AC loads. PV systems are becoming increasingly popular due to their simple installation, low maintenance, and cost-effective designs, a major focus for professional engineers.

PV-battery systems, which integrate battery storage with PV generation, are becoming more common as they approach "grid parity," meaning they are nearly as cost-effective as conventional energy sources (Kumar et al., 2017)-(Askarzadeh& dos Santos Coelho, 2015). However, conventional grid-connected PV systems are typically required to shut down in case of grid failure to ensure safety. A utility-interactive PV-battery system with energy storage provides an attractive alternative by delivering uninterrupted power to critical loads and managing peak demand (Kushwaha & Bhende, 2016)-(Kim & Parkhideh, 2018). In addition to supplying backup power, battery storage smooths out PV power fluctuations, aided by a bidirectional power converter that controls battery operation for both charging and discharging.

The power output of PV systems is highly sensitive to environmental factors, particularly irradiance and temperature (Dubey et al., 2013). Numerous Maximum Power Point Tracking (MPPT) methods have been developed to maximize power output under varying conditions by adjusting the converter's duty cycle (Abdulrazzaq et al., 2022). Various MPPT algorithms, including adaptive hill climbing (Xiao, 2003), perturb and observe (Elgendy et al., 2014), and variable step incremental conductance (Elgendy et al., 2012), aim to optimize voltage and current combinations for maximum power (Radjai et al., 2014). Additionally, nature-inspired algorithms such as genetic algorithms (Zagrouba et al., 2010), simulated annealing (El-Naggar et al., 2012), and particle swarm optimization (Khanna et al., 2015) have been introduced to address the limitations of conventional methods (Chou & Truong, 2020)-(Gouda et al., 2021).

Compared to other MPPT methods, the Fuzzy Logic Controller (FLC) approach provides a rapid response to changing conditions without needing additional hardware or detailed system parameter knowledge, making it adaptable for existing PV systems. It offers faster tracking speeds and improved steady-state accuracy (Zhang et al., 2017)-(Kottas et al., 2006). An FLC-based MPPT strategy, as described by (Yilmaz et al., 2018), reacts effectively under various environmental conditions. In most PV systems, a two-stage convertercomprising a boost converter and an inverterfacilitates MPPT and current management. However, this approach requires additional power components and can increase energy losses (Mechouma et al., 2012). Some studies have simplified PV systems by using a single inverter capable of both MPPT and power conversion, though this design requires a higher PV array bus voltage (Mechouma et al., 2012).

In recent years, Z-source inverters (ZSIs) have been proposed for PV systems (Ghahderijani & Dehkordi, 2020)-(KUMAR; BHATTACHARYA, 2015). A ZSI consists of two inductors and two capacitors arranged in an "X" configuration and includes an additional "shoot-through" time in its modulation to increase the PV array's voltage, enabling simultaneous MPPT and power conversion (Ghahderijani & Dehkordi, 2020)-(Singh et al., 2017). ZSIs are unique in their ability to adjust output AC voltage independently of input voltage, functioning as buck-boost inverters across a wide voltage range, a feature that traditional voltage-source and current-source inverters cannot achieve (PENG, 2003).

Voltage-source inverters (VSIs) are widely used for DC-AC power conversion in distributed power systems, AC motor drives, uninterruptible power supplies, and hybrid electric vehicles (AHMED et al., 2016). Three-level inverters, a variant of VSIs, offer several advantages over standard two-level VSIs, such as reduced device ratings, lower common-mode voltage, decreased dv/dt stress on power electronics, and reduced total harmonic distortion (THD) in the output current. However, the impedance network of three-level inverters introduces technical challenges, including reliability, efficiency, and increased control complexity (AHMED et al., 2016)-(BABAEI et al., 2016).

Among various techniques, the space vector pulse-width modulation (SVPWM) control strategy for neutral-point-clamped (NPC) inverters provides improved reliability and dynamic performance. Numerous studies have been conducted on SVPWM control strategies for NPC inverters (BEIG; NARAYANAN; RANGANATHAN, 2007)-(SAKTHISUDHURSUN; PANDIT; AWARE, 2015). This research proposes a streamlined SVPWM approach for three-level NPC ZSIs using a line-voltage coordinate system to minimize control complexity while achieving effective MPPT, addressing issues associated with complex operational regions and control intricacies.

2. DESCRIPTION OF THE SYSTEM

Our system comprises a photovoltaic (PV) array connected to a battery storehouse system via a DC link and a Z- source inverter. A battery bank, in confluence with a bidirectional DC- DC motor, stabilizes the DC link voltage, manages power inflow, and enhances power trustability. When the power generated by the PV array exceeds the cargo demand, the fat energy is stored in the batteries. Again, when the energy produced by the solar cells falls short of the needed cargo due to variations in temperature and irradiation, the battery supplies the fresh energy demanded. To optimize power birth from the PV array, we employ a maximum power point shadowing (MPPT) fashion grounded on fuzzy sense control (FLC). The inverter is connected to the grid through an LC sludge. The MPPT ensures that the energy gathered from the PV array is maintained at its maximum power point. Energy from either the battery or the PV system is also fitted into the grid via a three-position neutral-point clamped (NPC) Z- source inverter, which is controlled using a space vector palpitation rangemodulation (SVPWM) algorithm.

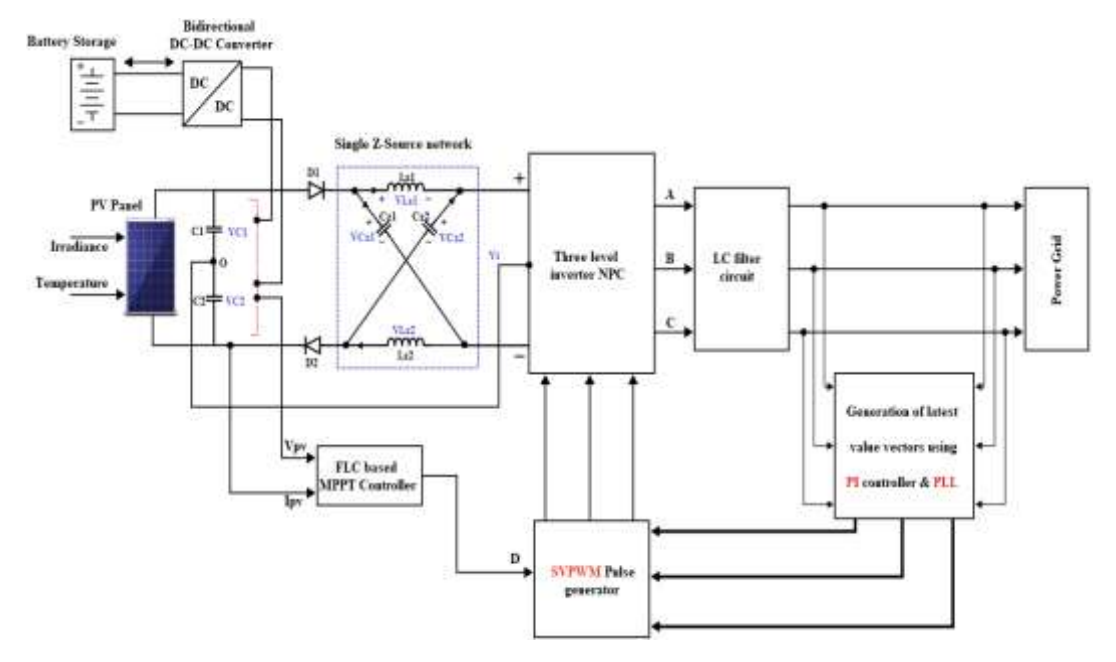


Figure 1. Structure of Z-source inverter three level PV grid-connected system with Bidirectional DC-DC Converter

2.1. DESCRIPTION OF THE SYSTEM

An comparable circuit for a single diode PV module is depicted in Figure 2. An equation (1) (BHUKYA; NANDIRAJU, 2020) expresses the output current of a PV module.

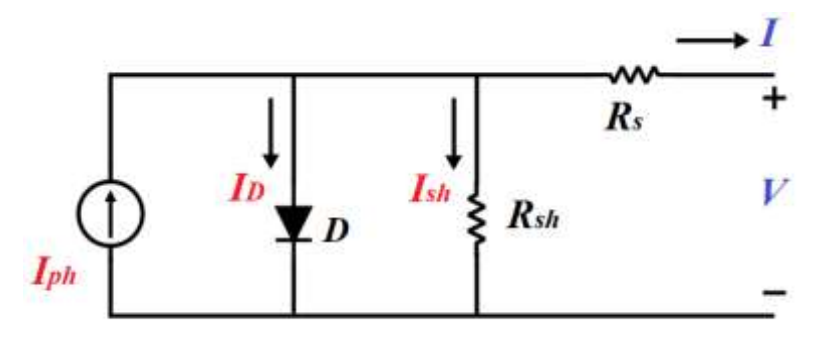


Figure 2. PV module equivalent circuit

$$I = I_{ph} - I_D - I_{sh}(1)$$

where Iis the output current of PV cell (A), I_{ph} is the photo generated current (A), I_{D} is the diode current (A) and I_{sh} is the shunt current (A).

 I_D represented the current flowing through the diode and was written as an equation (2) (AHMAD; SOBHAN; NAYAN, 2016)-(VISWAMBARAN; GHANI; ZHOU, 2016):

$$I_{D} = I_{0} \left(\exp \left(\frac{q(V + IR_{s})}{mkt_{c}} \right) - 1 \right)$$
 (2)

However, according to the model, the mathematical equation for the current in a PV cell is as follows (Radjai et al., 2014)-(Zagrouba et al., 2010):

$$I = I_{ph} - I_0 \left(\exp\left(\frac{q(V + IR_s)}{mkT_c}\right) - 1 \right) - \frac{V + IR_s}{R_{sh}}$$
 (3)

where I_0 is the saturation current of the diode (A), The elementary charge $(1.6\times10^{-19}~C)$ is represented by q, while the Boltzmann constant $(1.38\times10^{-23}~J/K)$ is represented by K, the diode quality factor is denoted by m, The PV cell output voltage is denoted by V, T_c is the cell's absolute temperature (K), R_s is the cell's series resistance (Ω) and R_{sh} is the cell's shunt resistance (Ω). The two most common types of PV modules are single-diode and double-diode variants. We can utilize the double-diode model to correctly create a solar panel model. Because of its simplicity and accuracy, the single-diode model is utilized in this research. The maximum power point current (I_{mp}) can be stated as follows:

$$I_{mp} = I_{ph} - I_0 \left(exp \left(\frac{q(V_{mp} + I_{mp}R_s)}{mkT_c} \right) - 1 \right) - \frac{V_{mp} + I_{mp}R_s}{R_{sh}}$$
(4)

The power at the maximum power point (P_{max}) is provided by:

$$P_{\text{max}} = V_{\text{mp}} \left\{ I_{\text{ph}} - I_0 \left(\exp \left(\frac{q(V_{\text{mp}} + I_{\text{mp}} R_s)}{mkT_c} \right) - 1 \right) - \frac{V_{\text{mp}} + I_{\text{mp}} R_s}{R_{\text{sh}}} \right\}$$
(5)

where I_{mp} is the highest possible panel current and V_{mp} is the highest possible panel voltage.

2.2. Proposed MPPT algorithm

FLC outperforms traditional algorithms, especially for complicated processes that cannot be evaluated using traditional quantitative approaches. It is both non-linear and adaptive, and it may be used in a variety of control applications. The framework of FLC is armed with four main essentials: fuzzifier, rule base, inference engine, and defuzzifier. The operation of the FLC structure may be easily understood from the illustration in Figure 3.

- 1) Fuzzification: In this technique, the crisp set utilized as input data is fuzzified utilizing linguistic variables, fuzzy linguistic words, and membership functions to change it into a fuzzy set. The most important aspect of fuzzy logic is that an arithmetic value does not have to be fuzzified using only one membership function. Membership functions include Triangular, Gaussian, Trapezoidal, Generalized Bell, and Sigmoid.
- 2) Rule Base: The rule base initiative governs the output variable. The matrix table characterizes the rule basis, which is an IF-THEN rule with an exact condition and conclusion. The two variables occupied along the axes are error and change in error, and the conclusions are included inside the table. In the rule base, the output of the membership function is well-defined as the least and extreme operator. The change in input often influences the fuzzy rule basis.

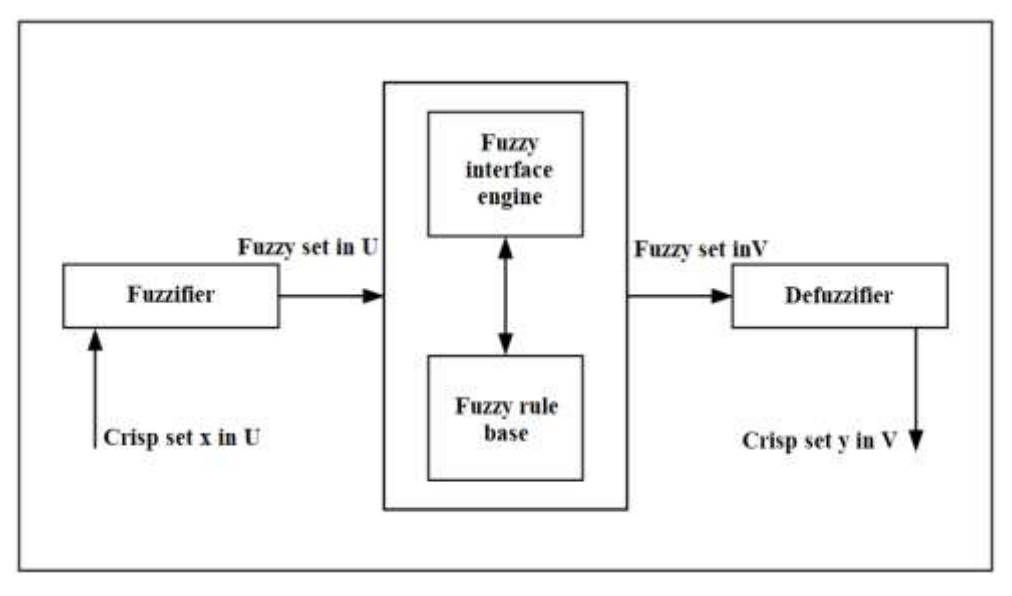


Figure 3. Fuzzy logic block

3) Defuzzification involves transforming the fuzzy set output from a fuzzy logic controller (FLC) into a precise, non-fuzzy control value. The fuzzy logic controller (FLC) provides a duty cycle output that controls the operation of the boost converter. Advantages of using an FLC include cost-effective implementation with affordable sensors and low-resolution analog-to-digital converters.

To sustain maximum power point (MPP), the error signal E should be zero at this point. The difference in the error signal, represented as ΔE , serves as an additional tuning factor for the fuzzy system. The signals E and ΔE are defined as follows:

$$E(i) = \frac{Ppv(i) - Ppv(i-1)}{Vpv(i) - Vpv(i-1)}$$

$$(6)$$

$$\Delta E = E(i) - E(i-1) \tag{7}$$

The table below represent the 25 fuzzy rules, where the L: low, H: high, VH: very high VL; very low, and N: null.

Table 1 Fuzzy ruls						
Ε/ΔΕ	VL	L	N	Н	VH	
VL	VH	VH	Н	VL	VL	
L	Н	Н	Н	VL	L	
N	Н	Н	N	L	L	
Н	Н	Н	L	L	VL	
VH	Н	Н	L	L	VL	

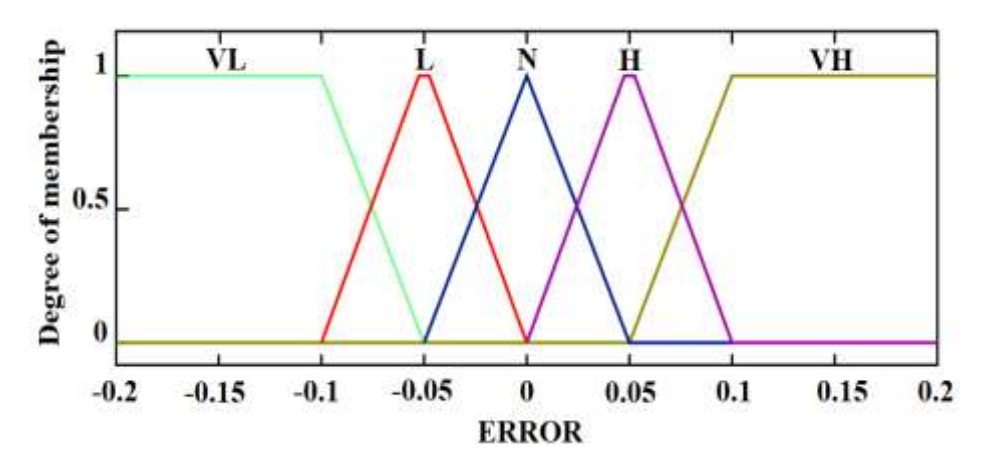


Figure 4. FLC's error membership function

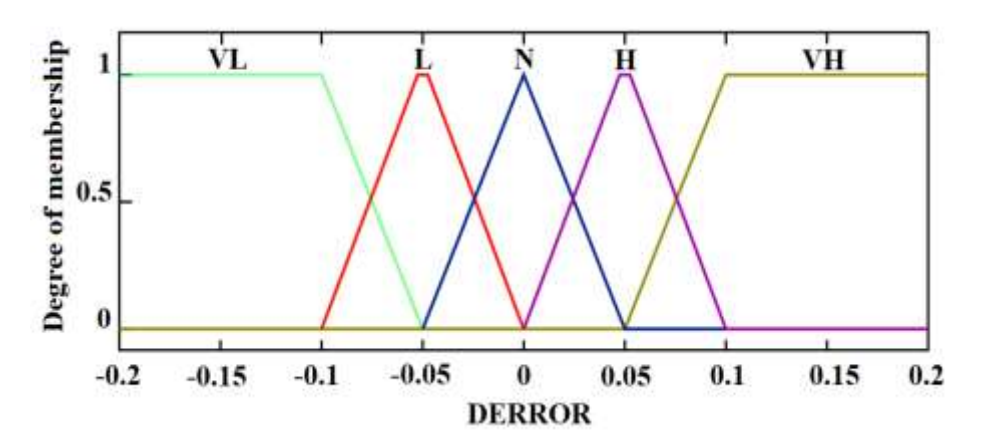


Figure 5. FLC error membership function change

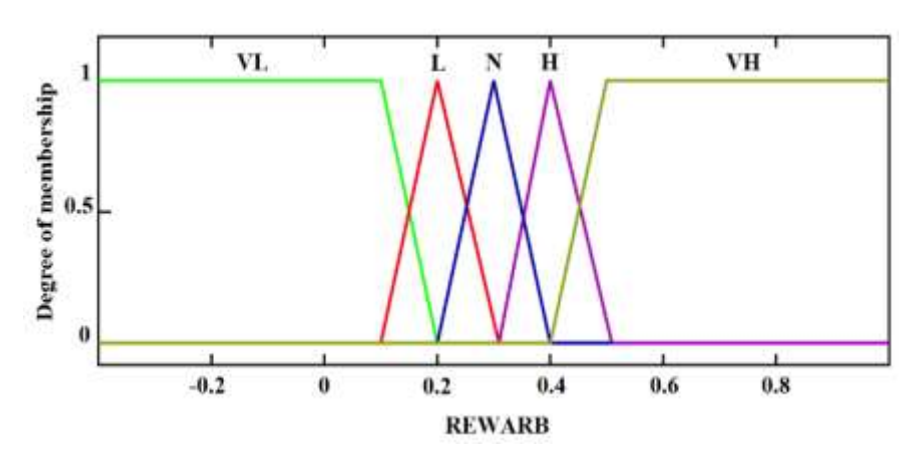


Figure 6. FLC's membership function output

2.3. Bidirectional converter and battery energy storage

A battery-based energy storage system is vital for a solar PV-powered microgrid. According to Reference (PONTES et al., 2021), various energy storage technologies are utilized in microgrids. Here, a battery system is linked to the DC bus via a bidirectional DC-DC converter (BDDC). The BDDC performs two main roles: (a) it controls the direction and amount of power exchange with the battery, and (b) it stabilizes the voltage and meets the power requirements of the DC link (TAVARES et al., 2017).

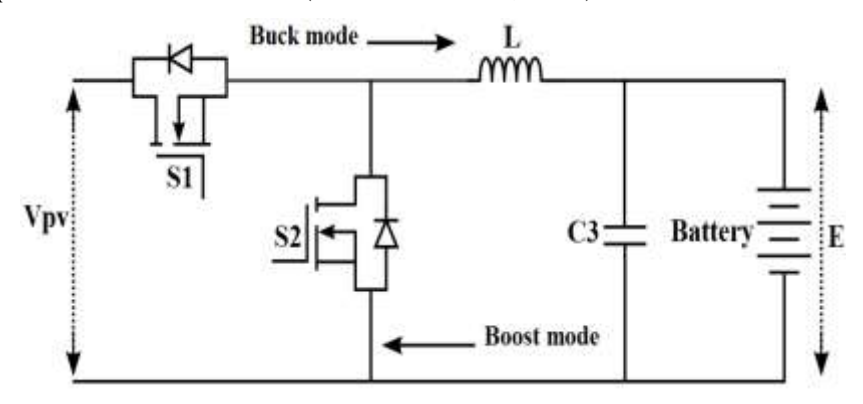


Figure 7. Bidirectional DC-DC Converter Circuit Diagram

Solar energy generation is directly proportional to solar irradiation, meaning that changes in irradiation levels directly affect power output. To mitigate the mismatch between energy generation and demand, bidirectional buck-boost battery storage technology can be employed. Figure 7 illustrates the operation of battery energy storage in relation to generation and demand.

During periods of over-generation (when PG>PL, where PG is the power generated by the PV panel and PL is the load power demand), the power output from the PV panel exceeds the demand. In this scenario, when gate S1 is activated, the MOSFET turns on, and the surplus energy is used to charge the battery, a process known as charging mode or buck mode. Conversely, during under-generation conditions (when PG<PL), the power output from the PV panel falls short of the load demand. In this case, when gate S2 is activated, the MOSFET is turned on, allowing both the battery and the PV panel to supply power to meet the load requirements. This operation is termed discharge mode or boost mode. Consequently, the overall output power remains relatively stable.

The design of inductors and capacitors on both the high-voltage and low-voltage sides is crucial for the system's proper operation. This design is informed by extensive research outlined in (SINGIRIKONDA et al., 2022). For continuous conduction mode operation, it is essential to select the larger of the two inductance values. Additionally, the capacitance values play a vital role in controlling voltage ripple on both the high-voltage and low-voltage sides.

3. The NPC Three-Level Z-Source Converters' Operation Principle

The structure of the three-level neutral-point clamped (NPC) Z-source inverter (ZSI) is illustrated in Figure 8. This design utilizes a two-port network to connect the three-level NPC inverter to the DC input source. The network includes two capacitors, Cz1=Cz2, and two inductors, Lz1=Lz2, with corresponding voltages VCz1=VCz2=VC and VLz1=VLz2=VL. The DC input sources, VC1 and VC2, are each set to half the PV voltage, Vpv/2. The neutral point is defined as the junction of the two DC input sources and is connected to the neutral point of the three-level NPC inverter. Each phase arm operates with three switching states: "1," "0," and "-1." In switching state "1," the two upper switches in the phase arm are activated; in state "-1," the two lower switches are activated; and in state "0," the two inner switches are activated.

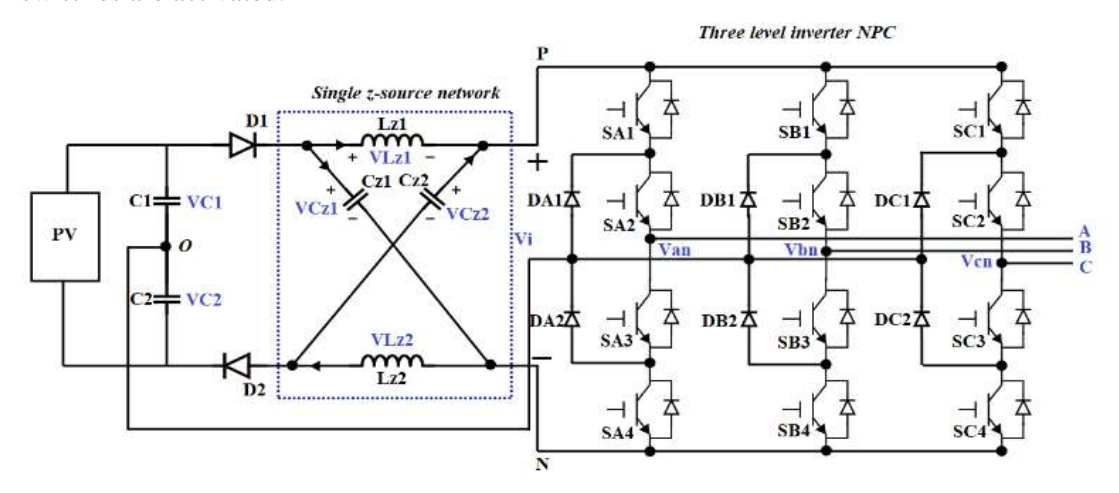


Figure 8. The three-level NPC ZSC topology

The system is in an upper shoot-through (UST) state, labeled as "U," when the three upper switches (e.g., SA1, SA2, and SA3) are activated. Conversely, if all three lower switches are turned on, this condition is called down shoot-through (DST) and is marked by the label "D." Table 2 outlines the different states of this configuration. Figures 9, 10, and 11 illustrate three distinct operating modes: non-shoot-through, UST, and DST.

Table 2 Various states and output voltages				
Time Duration	MODE	Turn-On Device	Output Voltage	
Tsh_N	1	SX1, SX2, D1, D2	Vi/2	
Tsh_N	0	SX2, SX3, D1, D2	0	
Tsh_N	-1	SX3, SX4, D1, D2	-Vi/2	
Tsh_U	U	SX1, SX2, SX3, D1	0 or -Vi	
Tsh_D	D	SX2, SX3, SX4, D2	0 or Vi	

Table 2 Various states and output voltages

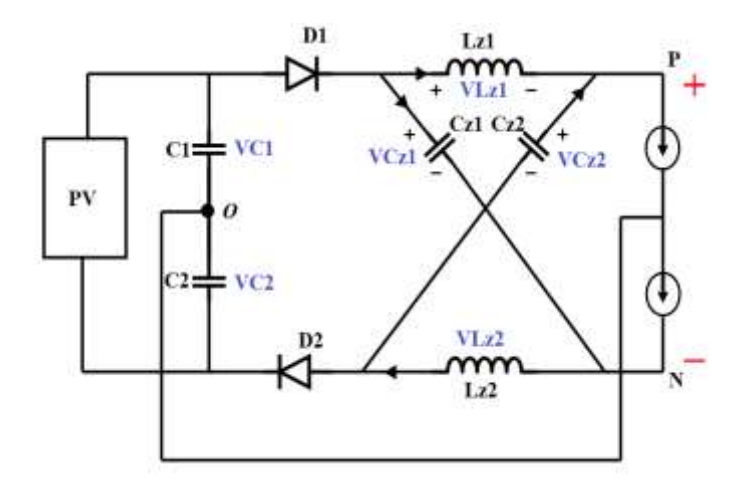


Figure 9 Nonshoot-through

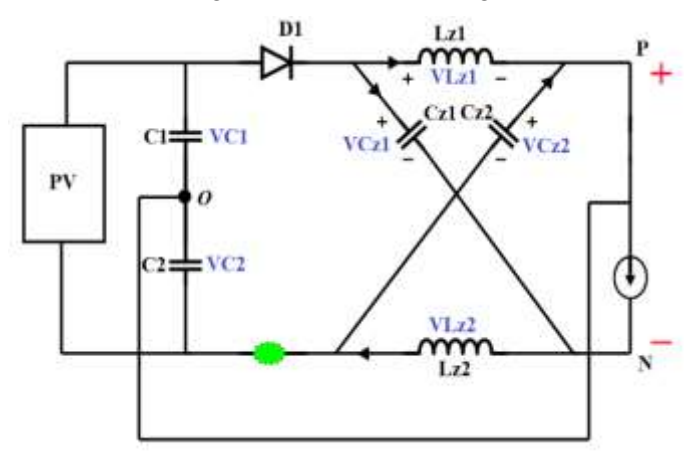


Figure 10 Up shoot-through

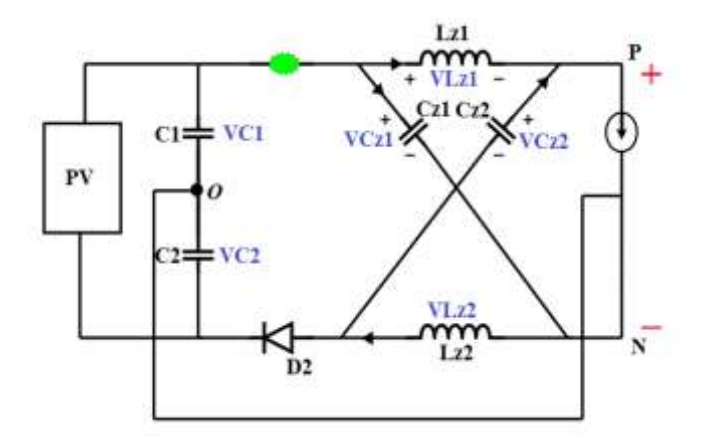


Figure 11 Down shoot-through

Nanotechnology Perceptions Vol. 20 No.6 (2024)

 $T_{sh}u$ is the time length of UST status, while $T_{sh}D$ is the time duration of DST state. In order to eliminate the output voltage harmonic components, $T_{sh}u$ should normally be equal to $T_{sh}D$.

$$T_{sh}u = T_{sh}u = T_{sh} \tag{8}$$

Based on the average inductor voltage, the relationship between the capacitor voltage (V_C) and the input voltage (V_{dc}) for a fixed switching period may be described as

$$V_{c} = \frac{T_{S} - T_{sh}}{T_{S} - 2T_{sh}} .2V_{dc} = \frac{\left(1 - \frac{T_{sh}}{T_{S}}\right)}{\left(1 - \frac{2T_{sh}}{T_{c}}\right)} .2V_{dc} = \frac{1 - D}{1 - 2D} .2V_{dc}$$
(9)

The duty ratio of the shoot through states is defined as $D = (T_{sh}/T_S)$. The output voltage V_i may be obtained in the non shoot-through state.

$$V_{i} = \frac{1}{1 - 2D} 2V_{dc} \tag{10}$$

The three output voltages can now be depicted as well

$$V_{P} = \frac{V_{dc}}{1 - 2D} \tag{11}$$

$$V_0 = 0 \tag{12}$$

$$V_{N} = -\frac{V_{dc}}{1 - 2D} \tag{13}$$

where V_P represents the output phase voltage when only two up switches of a phase arm are switched on and V_N represents the output phase voltage when only two down switches of a phase arm are turned on When two inner switches of a phase arm are switched on, V_0 expresses the output phase voltage.

And the output phase voltage U_x may be calculated as

$$U_x = M \cdot \frac{V_{dc}}{1 - 2D} = MH \cdot V_{dc}, \qquad x = a, b, c,$$
 (14)

where M denotes the modulation coefficient and H = 1/(1-2D) denotes the booster ratio.

4. SVPWM Modulation Implementation

As shown in Figure 12, a three-level inverter includes 12 switches (4 per bridge arm) that operate in a specific pattern to generate 27 distinct space voltage vectors. By using linear combinations of these vectors, the inverter can approximate the reference voltage vector more accurately. Building on the conventional space vector pulse width modulation (SVPWM), a new SVPWM algorithm can be developed specifically for a single Z-source three-level inverter by strategically inserting upper and lower shoot-through states. Generally, this process involves identifying regions, determining state sequences, calculating switching times (QU et al., 2011), inserting shoot-through vectors, and assigning timing for

Nanotechnology Perceptions Vol. 20 No.6 (2024)

each state.

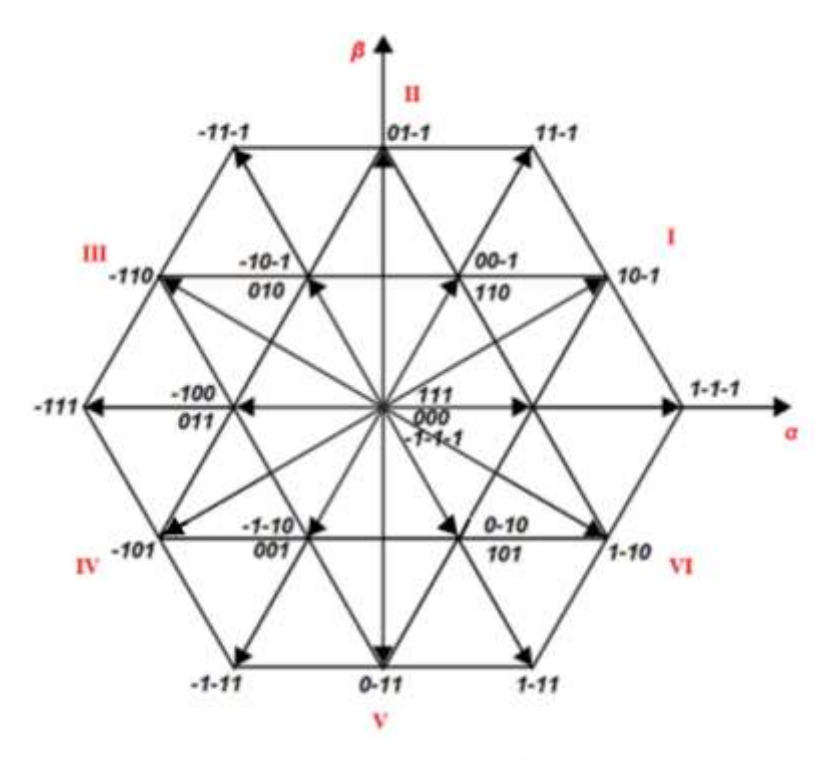


Figure 12 Three-level inverter basic space vectors

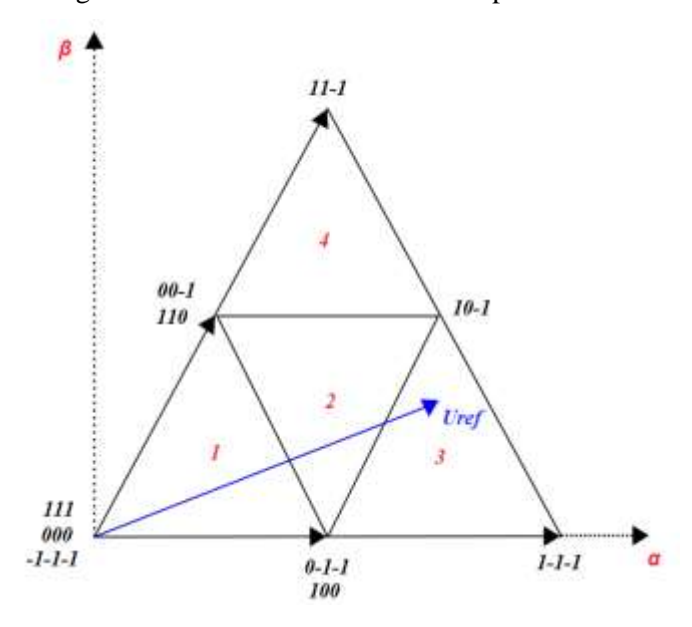


Figure 13 Space voltage vectors in Zone I

Inserting a shoot-through vector. Upper or lower shoot-through vectors in the computed state sequence should fulfill the symmetric distribution. The insertion of shoot-through states *Nanotechnology Perceptions* Vol. 20 No.6 (2024)

should not affect the volt-sec balance, which means that the insertion should not change the output-voltage state of the bridge arms; the durations of upper and lower shoot-through states should be equal to ensure output voltage balance; and the insertion should not increase device commutations. In one section, Figure 14. depicts the modulation sequence of a Z-source three-level inverter.

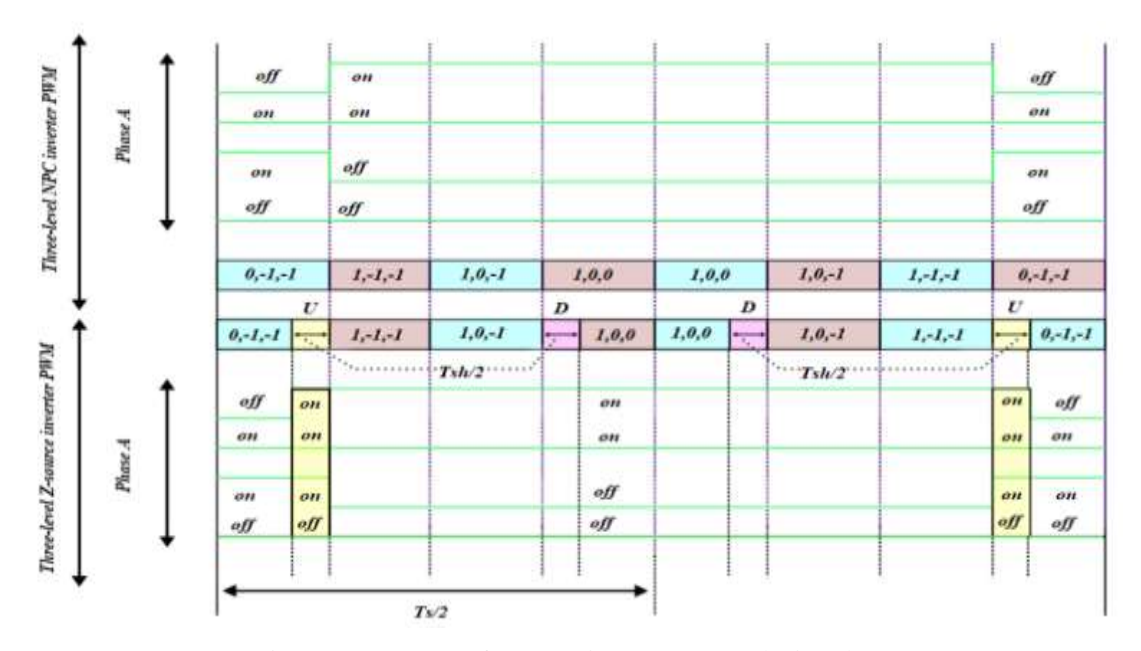


Figure 14 Strategy for Insertion (Zone I and triangle 3)

Introducing shoot-through states affects both the boost efficiency and the levels of output harmonic distortion, as well as the switching losses. For the space voltage vectors presented in Figure 12. the derived optimal voltage Uref, as shown in Figure 13. is located in Zone I and triangle 3. Assume the initial switch state is "0 1 1," which indicates that SA2, SA3, SB3, SB4, SC3, and SC4 are all switched on:

(1) At t = t1, switch state "0 1 1" to "1 1 1" (for phase A, SA is changed from "0" to "1"), and the UST might be inserted in phase A by beforehand turning on the switch "SA1," as illustrated in Figure 9. (SA1, SA2, and SA3 are in the ON state, while SA4 is in the OFF state).

The switch states for phases B and C stay unaltered during this insertion, so satisfying the "volt-second" concept.

- (2) At t = t2, convert state "1 1 1" to "1 0 1" (for phase B, shift SB from "1" to "0"). If the UST has already been inserted in phase B, the switch state of phase A might be retained as "1," but the switch state of phase C should be clamped from "1" to "0," which would destroy the "volt-second" state, therefore this insertion should be removed.
- (3) At t=t3, convert state "1 0 1" to "1 0 0" (for phase C, SC is changed from "1" to "0").

Figure 9. shows how DST might be inserted into phase C by repeatedly turning on the switch "SC4" (SC2, SC3, and SC4 are ON while SC1 are OFF). The switch states for phases A and B stay identical during this insertion, so satisfying the "volt-second" concept.

If the reference vector is located in Zone I within triangle 3, the UST and DST can be positioned within the range of the associated zero vector for interaction. Thus, the condition $T_{sh}u = T_{sh}D$ can assure the balance of the UST and DST status.

Figure 13. clearly shows that both the up and down shoot-through states enhance the output voltage.

5. Simulation Results

A three-level Space Vector Pulse Width Modulation (SVPWM)-based Neutral-Point Clamped (NPC) Z-source inverter (ZSI) with a single impedance network is analyzed for grid-connected photovoltaic (PV) applications and integration with a bidirectional DC-DC converter. The simulation parameters are outlined in Table 3. The PV panel's DC output voltage is boosted to the required level and converted to AC for grid integration. Using an appropriate inverter control strategy, the power is fed into the grid at a unity power factor. The influence of irradiance variation at a constant temperature of 25°C is examined using MATLAB/SIMULINK simulation.

The PV panel's DC output voltage (258.53V, as shown in Figure 15) is raised to the necessary level and converted to an AC peak voltage of 400V (as depicted in Figures 17 and 18) to feed the grid. Figure 15 illustrates that when the irradiance increases from 500 W/m² to 1000 W/m² between 1.9 and 4.8 seconds, the power output rises from 1080W to 2130W. As the irradiance decreases from 1000 W/m² to 750 W/m² between 4.8 and 7.5 seconds, the PV panel's power output drops from 2130W to 1613.5W. Similarly, when the irradiance reduces further from 750 W/m² to 300 W/m² between 7.5 and 10 seconds, the power output decreases from 1613.5W to 644.15W.

The rated power output (from the datasheet) is 2132W, and the steady-state power at 1000 W/m² is 2130W, as shown in Figure 15, yielding a Maximum Power Point Tracking (MPPT) efficiency of 99.90%. Voltage and current levels fluctuate proportionally with the changes in power output.

Table 3 Parameters for simulation			
Parameters	Values		
L_{Z1}	0.5 mH		
L_{Z2}	0.5 mH		
C_{Z1}	1 mF		
C_{Z2}	1 mF		
T_S	60 μs		
C1, C2	500 μF		
Lgrid	1 mH		

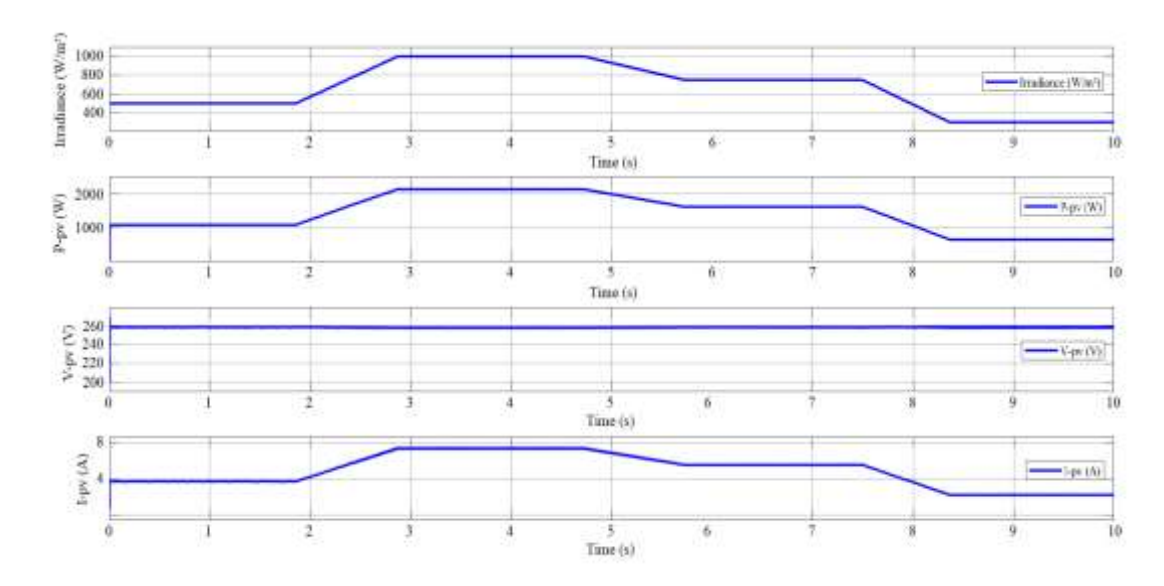


Figure 15 Simulation results of the photovoltaic (Irradiance, P-pv, V-pv, I-pv)

The analysis in Figure 16 illustrates how excess power is managed when generation exceeds demand (over-generation) between 1.9 and 4.8 seconds, where PG>PL. During this period, the battery charges, raising its state of charge (SOC) from 50% to approximately 50.165%, accompanied by an increase in battery voltage and a negative battery current as current flows into the battery. Conversely, when load demand exceeds generation (under-generation) from 4.8 to 10 seconds, the battery and photovoltaic (PV) panel jointly supply power to the load. The battery discharges, with SOC decreasing from 50.165% to 50.28% between 4.8 and 7.5 seconds, and further from 50.28% to 50.221% from 7.5 to 10 seconds. This results in a drop in battery voltage and a positive battery current flowing out to the system. This arrangement minimizes power and voltage fluctuations despite changes in irradiance.

The battery serves to stabilize output power, ensuring a relatively constant supply with less volatility than the input. To achieve the required AC output voltage, the Z-Source Inverter (ZSI) maintains the desired boosted DC link voltage. As shown in Figure 15, even with variations in irradiance, the output peak voltage remains steady (see Figures 17 and 18). The battery's charging and discharging cycles, which span 5–10 cycles, effectively moderate the power supplied to the ZSI. During the over-generation period (1.9 to 5.7 seconds), the shoot-through duty ratio decreases, while it increases during under-generation (5.7 to 10 seconds).

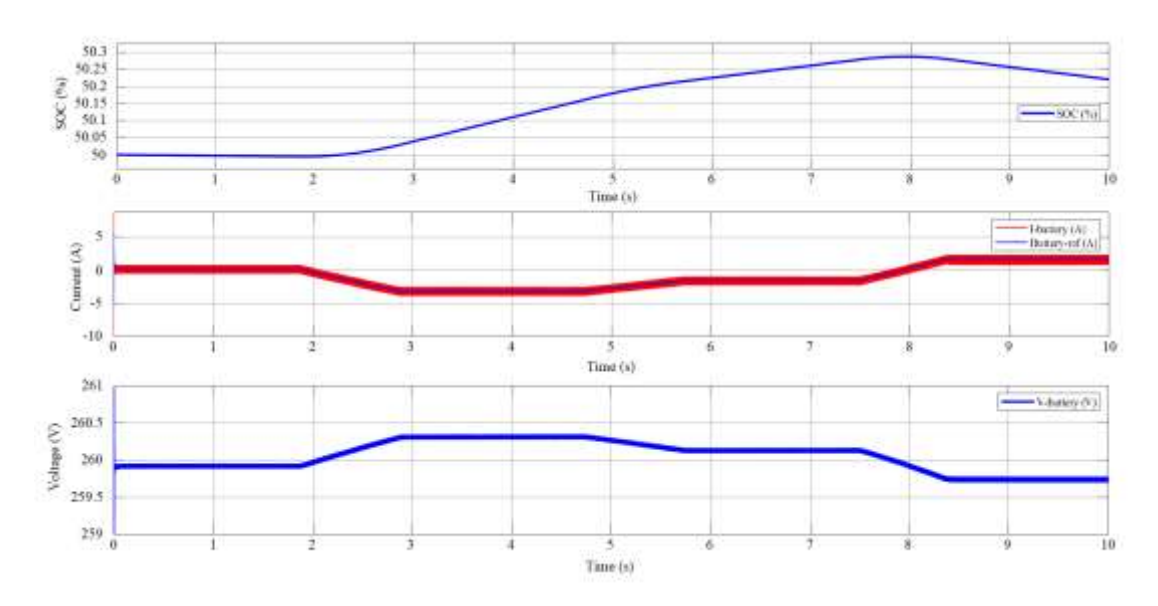


Figure 16 Simulation results of the battery (State of charge of battery (SOC), battery current, battery voltage)

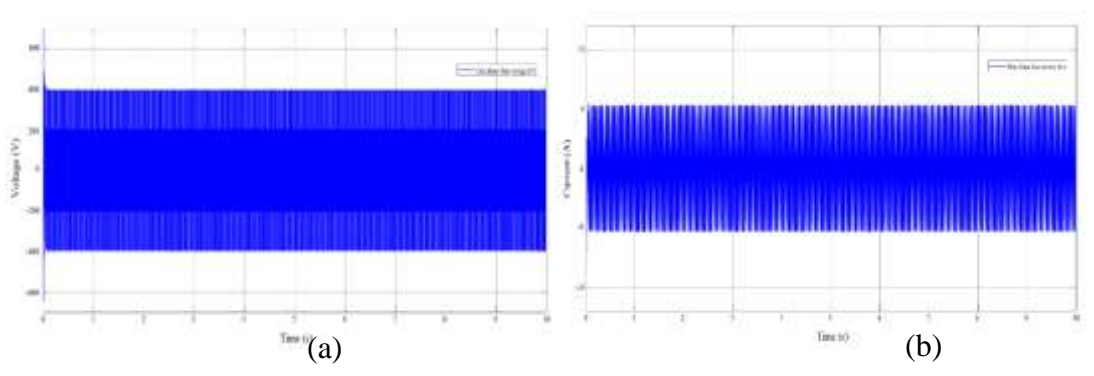


Figure 17 (a) one phase line voltage (b) One phase line current

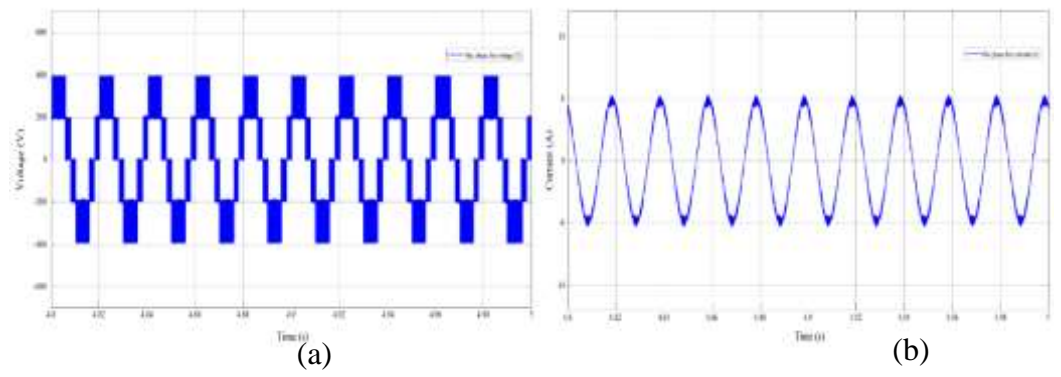


Figure 18 (a) one phase line voltage (b) One phase line current

The current waveform in Figure 19 shows that current is supplied to the grid with an almost *Nanotechnology Perceptions* Vol. 20 No.6 (2024)

unity power factor, meeting the required AC output voltage while the grid voltage remains constant. The level of grid current varies with irradiance changes. Figure 20(a) illustrates how grid current is affected by fluctuations in solar radiation, with a gradual decrease in peak grid current without any phase shift. In Figure 20(b), a phase voltage waveform and phase net current waveform are displayed at a solar irradiance of 1000 W/m², demonstrating that the controller can regulate net current, grid voltage, frequency, and phase to maintain the desired power factor interconnection, as seen in Figure 21. The grid current has a low harmonic distortion rate, with a THD value of only 1.93%, which minimally impacts the power grid.

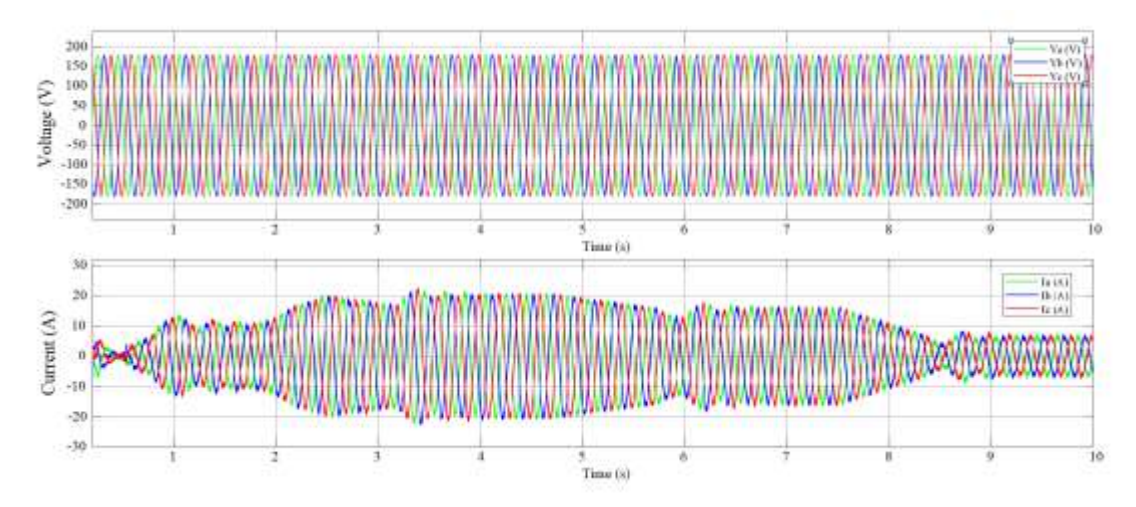


Figure 19 Dynamic response of the system to step change in solar irradiance, of grid voltage and current

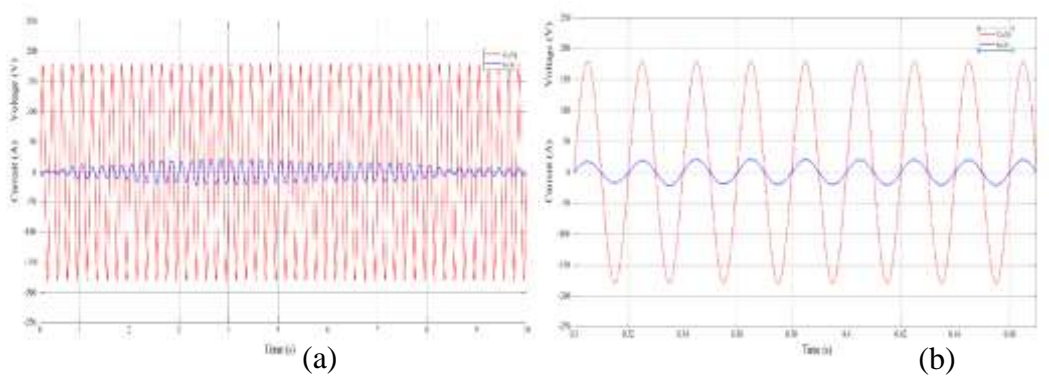


Figure 20 Dynamic response of grid voltage and current: (a) of the step change in solar irradiance (b) in steady-state solar irradiance condition, with 1000-W/m2 solar irradiance

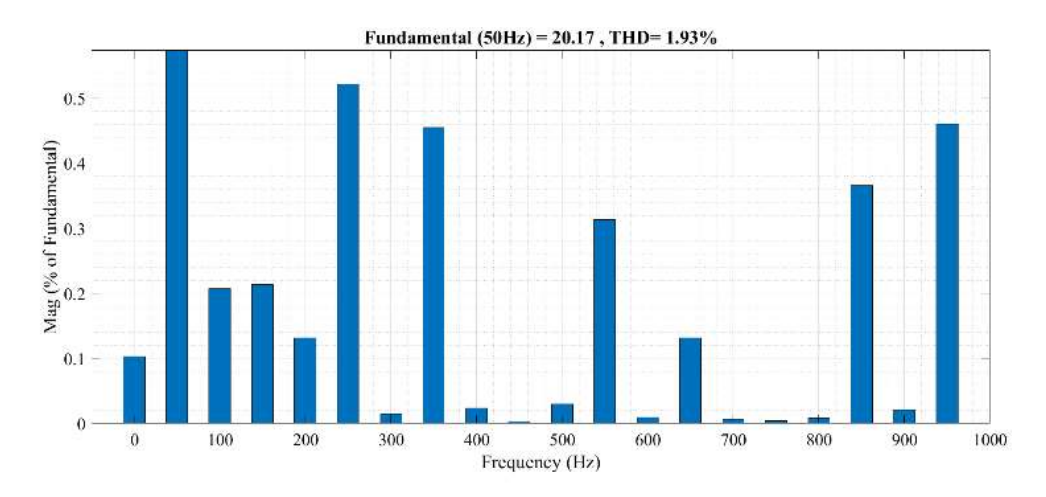


Figure 21 FFT analysis of steady state of current fed into grid

6. CONCLUSION

A photovoltaic (PV) system with MPPT control and integrated battery energy storage has been successfully designed and simulated. This system incorporates a bidirectional DC-DC converter and a modified three-level neutral-point clamped (NPC) Z-source inverter, utilizing space vector pulse width modulation (SVPWM) as confirmed by modeling and experimental results. By combining the functions of boosting, inverting, and maximum power point tracking (MPPT) into a single power stage, the system reduces the need for additional switching devices, eliminating the requirement for a separate boost converter at the inverter output. This integration not only lowers costs and reduces power losses but also enhances system reliability by improving output voltage and current control. Additionally, issues related to capacitor balancing and common-mode voltage in a Z-source diode-clamped multilevel inverter are effectively managed. Overall, the NPC three-level Z-source inverter (ZSI) with integrated battery storage provides enhanced performance with reduced hardware costs and complexity.

References

- 1. Zha, Y., Lin, J., Li, G., & Wang, Y. (2021). Analysis of inertia characteristics of photovoltaic power generation system based on generalized droop control. IEEE Access, 9, 37834–37839.
- 2. Mahmud, K., Azam, S., Karim, A., Zobaed, S., Shanmugam, B., & Mathur, D. (2021). Machine learning based PV power generation forecasting in alice springs. IEEE Access, 9, 46117–46128.
- 3. Kumar, N. M., Kumar, M. R., Rejoice, P. R., & Mathew, M. (2017). Performance analysis of 100 kWp grid connected Si-poly photovoltaic system using PVsyst simulation tool. Energy Procedia, 117, 180–189.
- 4. Askarzadeh, A., & dos Santos Coelho, L. (2015). A novel framework for optimization of a grid independent hybrid renewable energy system: A case study of Iran. Solar Energy, 112, 383–396. https://doi.org/10.1016/j.solener.2014.12.013

- 5. Kushwaha, P. C., & Bhende, C. N. (2016). Single-phase rooftop photovoltaic based grid-interactive electricity system. 2016 IEEE Annual India Conference (INDICON), 1–6.
- 6. Kim, N., & Parkhideh, B. (2018). Control and operating range analysis of an AC-stacked PV inverter architecture integrated with a battery. IEEE Transactions on Power Electronics, 33(12), 10032–10037.
- 7. Dubey, S., Sarvaiya, J. N., & Seshadri, B. (2013). Temperature dependent photovoltaic (PV) efficiency and its effect on PV production in the world–a review. Energy Procedia, 33, 311–321.
- 8. Abdulrazzaq, A. K., Bognár, G., & Plesz, B. (2022). Accurate method for PV solar cells and modules parameters extraction using I–V curves. Journal of King Saud University Engineering Sciences, 34(1), 46–56. https://doi.org/10.1016/j.iksues.2020.07.008
- 9. Xiao, W. (2003). A modified adaptive hill climbing maximum power point tracking (MPPT) control method for photovoltaic power systems, Master's thesis. July, 103.
- 10. Elgendy, M. A., Zahawi, B., & Atkinson, D. J. (2014). Operating characteristics of the P&O algorithm at high perturbation frequencies for standalone PV systems. IEEE Transactions on Energy Conversion, 30(1), 189–198.
- 11. Elgendy, M. A., Zahawi, B., & Atkinson, D. J. (2012). Assessment of the incremental conductance maximum power point tracking algorithm. IEEE Transactions on Sustainable Energy, 4(1), 108–117.
- 12. Radjai, T., Rahmani, L., Mekhilef, S., & Gaubert, J. P. (2014). Implementation of a modified incremental conductance MPPT algorithm with direct control based on a fuzzy duty cycle change estimator using dSPACE. Solar Energy, 110, 325–337.
- 13. Zagrouba, M., Sellami, A., Bouaïcha, M., & Ksouri, M. (2010). Identification of PV solar cells and modules parameters using the genetic algorithms: Application to maximum power extraction. Solar Energy, 84(5), 860–866. https://doi.org/10.1016/j.solener.2010.02.012
- 14. El-Naggar, K. M., AlRashidi, M. R., AlHajri, M. F., & Al-Othman, A. K. (2012). Simulated annealing algorithm for photovoltaic parameters identification. Solar Energy, 86(1), 266–274.
- 15. Khanna, V., Das, B. K., Bisht, D., & Singh, P. K. (2015). A three diode model for industrial solar cells and estimation of solar cell parameters using PSO algorithm. Renewable Energy, 78, 105–113.
- 16. Chou, J.-S., & Truong, D.-N. (2020). Multiobjective optimization inspired by behavior of jellyfish for solving structural design problems. Chaos, Solitons & Fractals, 135, 109738.
- 17. Gouda, E. A., Kotb, M. F., & El-Fergany, A. A. (2021). Jellyfish search algorithm for extracting unknown parameters of PEM fuel cell models: Steady-state performance and analysis. Energy, 221, 119836.
- 18. Zhang, J., Deng, Z., Choi, K.-S., & Wang, S. (2017). Data-driven elastic fuzzy logic system modeling: Constructing a concise system with human-like inference mechanism. IEEE Transactions on Fuzzy Systems, 26(4), 2160–2173.
- Kottas, T. L., Boutalis, Y. S., & Karlis, A. D. (2006). New maximum power point tracker for PV arrays using fuzzy controller in close cooperation with fuzzy cognitive networks. IEEE Transactions on Energy Conversion, 21(3), 793–803. https://doi.org/10.1109/TEC.2006.875430
- 20. Yilmaz, U., Kircay, A., & Borekci, S. (2018). PV system fuzzy logic MPPT method and PI control as a charge controller. Renewable and Sustainable Energy Reviews, 81(August 2017), 994–1001. https://doi.org/10.1016/j.rser.2017.08.048
- 21. Mechouma, R., Azoui, B., & Chaabane, M. (2012). Three-phase grid connected inverter for photovoltaic systems, a review. 2012 1st International Conference on Renewable Energies and Vehicular Technology, REVET 2012, 37–42. https://doi.org/10.1109/REVET.2012.6195245
- 22. Ghahderijani, M. M., & Dehkordi, B. M. (2020). Comprehensive robust and fast control of \$ Z \$-Source-Inverter-Based interior permanent magnet synchronous motor drive system. IEEE

- Transactions on Industrial Electronics, 68(12), 11783–11793.
- 23. Singh, S. A., Carli, G., Azeez, N. A., & Williamson, S. S. (2017). Modeling, design, control, and implementation of a modified Z-source integrated PV/grid/EV DC charger/inverter. IEEE Transactions on Industrial Electronics, 65(6), 5213–5220.
- 24. KUMAR, A.; BHATTACHARYA, A. Three level Z source inverter based photovoltaic power conversion systems. IECON 2015-41st Annual Conference of the IEEE Industrial Electronics Society. Anais...IEEE, 2015.
- 25. PENG, F. Z. Z-source inverter. IEEE Transactions on industry applications, v. 39, n. 2, p. 504–510, 2003.
- 26. AHMED, I. et al. Simplified Space Vector Modulation Techniques for Multilevel Inverters. IEEE Transactions on Power Electronics, v. 31, n. 12, p. 8483–8499, 2016.
- 27. BABAEI, E. et al. Developed embedded switched-Z-source inverter. IET Power Electronics, v. 9, n. 9, p. 1828–1841, 2016.
- 28. BEIG, A. R.; NARAYANAN, G.; RANGANATHAN, V. T. Modified SVPWM algorithm for three level VSI with synchronized and symmetrical waveforms. IEEE transactions on industrial electronics, v. 54, n. 1, p. 486–494, 2007.
- 29. SAKTHISUDHURSUN, B.; PANDIT, J. K.; AWARE, M. V. Simplified three-level five-phase SVPWM. IEEE Transactions on Power Electronics, v. 31, n. 3, p. 2429–2436, 2015.
- 30. BHUKYA, L.; NANDIRAJU, S. A novel photovoltaic maximum power point tracking technique based on grasshopper optimized fuzzy logic approach. International journal of hydrogen energy, v. 45, n. 16, p. 9416–9427, 2020.
- 31. AHMAD, T.; SOBHAN, S.; NAYAN, F. Comparative Analysis between Single Diode and Double Diode Model of PV Cell: Concentrate Different Parameters Effect on Its Efficiency. n. March, p. 31–46, 2016.
- 32. VISWAMBARAN, V. K.; GHANI, A.; ZHOU, E. Modelling and simulation of maximum power point tracking algorithms & review of MPPT techniques for PV applications. 2016 5th international conference on electronic devices, systems and applications (ICEDSA). Anais...IEEE, 2016.
- 33. PONTES, L. R. B. et al. Optimal allocation of energy storage system in distribution systems with intermittent renewable energy. IEEE Latin America Transactions, v. 19, n. 02, p. 288–296, 2021.
- 34. SINGIRIKONDA, S. et al. Adaptive control-based Isolated bi-directional converter for G2V& V2G charging with integration of the renewable energy source. Energy Reports, v. 8, p. 11416–11428, 2022.
- 35. TAVARES, S. E. et al. Bidirectional power converter with adaptive controller applied in direct-current microgrid voltage regulation. 2017 IEEE 8th International Symposium on Power Electronics for Distributed Generation Systems, PEDG 2017, p. 0–5, 2017.
- 36. QU, K. et al. A SVPWM control strategy for NPC three-level inverter. 2011 IEEE power engineering and automation conference. Anais...IEEE, 2011.